Copied From Los Alamos
National Laboratory Archives

712888

A-91-011
73-2
MP-DO

# PION CLINICAL PHYSICS PROGRAM

I. ORGANIZATION OF CLINICAL PHYSICS SECTION

II. PROGRESS

III. FUTURE WORK

REPOSITORY LANL RC
COLLECTION MP DO
BOX No.
FOLDER

FILE BARCODE
00133500

COPIED FOR
HSPT

00133500.001

1087355

# I. ORGANIZATION OF UNM PHYSICS STAFF AT LOS ALAMOS

Al Smith, Ph.D.
Chief Physicist

1. Clinical Applications
2. Therapy Liaison
3. MP-3 Liaison
4. Technical Liaison

## Treatment Planning

Eric Gelfand, Ph.D.
Steve Simon, M.S.

1. Bolus Design
2. Collimator Design
3. Dose Distributions
4. Site Doses
5. Patient Dosimetry
6. CT Applications

## Control Room

Roy Slice
Lyn Jackson

1. Patient Treatment
2. Dose Calculation
3. Patient Records
4. Equipment Design and Fabrication

## Research & Development

Ken Hogstrom, Ph.D.
Assistant Chief Physicist

1. Developmental Dosimetry
2. In-Vivo Systems
3. Visualization
4. Software

John Somers, M.S.

1. Electronics Design and Fabrication
2. PIP Systems
3. Treatment Control Systems
4. Equipment Maintenance

COPIED FOR
HSPT

00133500.002

1087356

## II. PROGRESS

1. Automated dosimetry data-acquisition and analysis system: Provides for automatic measurement of one, two, and three dimensional dose distributions in a water phantom, produces data plots on scope during scanning and produces hard copy of data and plots.

2. Characterization of large variety of pion therapy beams. The beams include three different pion momenta with three beam sizes for each momenta and fourteen different stopping pion configurations for each beam size.

3. Measured the effect of various inhomogeneities in pion therapy beams, and the ability of compensating bolus to correct for these effects.

4. Measured the linear pion stopping power ratios (versus water) and linear attenuation coefficients using CT scanners for a variety of tissue simulating materials. This data is used in treatment planning programs.

5. Developed treatment planning methods and computer algorithms for pions. This includes the use of CT data for compensation for anatomical and geometric inhomogeneities.

6. Developed methods for the design and fabrication of compensating bolus and collimators for pion therapy.

7. Developed methods and designed apparatus for set-up, immobilization, simulation, transport, and treatment of pion patients.

8. Developed methods of calculating pion isodose distributions in water phantoms which includes the effects of multiple pion scattering and collimation.

9. Developed methods of calculating patient isodose distributions which includes the patient CT data, bolus, and beam data derived from measurements and calculations.

10. Developed methods of in vivo dosimetry which includes ionization chambers, TLD, and aluminum activation to measure the total dose and the high LET dose.

11. Performed feasibility studies on method of imaging stopping pions in patients using positron emission.

12. Developed a multi-chamber dosimetry system which utilizes an array of chambers to rapidly perform dosimetry measurements in pion beams so that less beam time is required.

13. Developed focused beams for use in dynamic scanning of pion patients to improve the sparing of normal tissues. Developed methods for dynamic treatments.

COPIED FOR
HSPT



1087357

## III. FUTURE WORK

1. Installation and interfacing of new CT scanner.
2. Investigation of relationship between CT numbers and pion linear stopping powers for a variety of tissue equivalent materials.
3. Development and implementation of focused beams and treatment systems for the treatment of patients using dynamic scanning.
4. Development of improved patient immobilization devices and set-up techniques.
5. Continuing investigation of position emission visualization.
6. Calculations and experiments to explain the complicated energy deposition processes in ionization chambers due to stopping pions.
7. Expand and improve the multi-chamber dosimetry system.
8. Investigate the properties of new materials which may be suitable for bolus.
9. Conduct intercomparisons at other charged particle therapy facilities in the USA, Canada, Europe, and Japan using a tissue equivalent calorimeter and ionization chambers. Write a protocol for charged particle dosimetry.

COPIED FOR
HSPT

1087358

00133500.004

# Dosimetry of pion therapy beams

Alfred R. Smith, Isaac I. Rosen, Kenneth R. Hogstrom, Richard G. Lane, and Charles A. Kelsey

*University of New Mexico, Cancer Research and Treatment Center, Albuquerque, New Mexico 87131*

Howard I. Amols, Chaim Richman, Peter A. Berardo, Jerome A. Helland, Richard S. Kittell, Michael A. Paciotti, and James N. Bradbury

*Los Alamos Scientific Laboratory of the University of California, Los Alamos, New Mexico 87545*

COPIED FOR HSPT

FILE BARCODE 00133501

Cellular, animal, and human radiobiology studies are in progress at the Los Alamos Meson Physics Facility as part of a joint University of New Mexico and Los Alamos Scientific Laboratory pion therapy project. To support these activities, dosimetry has been performed on many different pion beam configurations. The effect of both static and dynamic momentum spreaders and of collimators on beam profiles, depth-dose distributions, and peak-to-plateau ratios have been studied. The absorbed dose is obtained by the application of Bragg–Gray cavity theory to ionization chamber measurements. Calculations have been made for the effective $W$ values and average mass-stopping-power ratios needed for the Bragg–Gray equation. Kerma corrections are applied to transform the dose from the chamber wall to dose in muscle.

## I. INTRODUCTION

Negative $\pi$ meson (pion) radiotherapy programs are being developed at the following facilities: Los Alamos Meson Physics Facility (LAMPF) and Stanford University in the USA; TRIUMPF, Vancouver, Canada; SIN near Zurich in Switzerland; and Dubna in the USSR. At all these facilities pion beam intensities are still rather low but sufficiently high to perform beam physics and dosimetry studies together with some selected radiobiological investigations. Only at LAMPF are pion dose rates high enough to permit the human radiobiological studies now in progress.

Pions offer the possibility of improving the therapeutic ratio between malignant tumors and normal tissues by having highly localized dose distributions and a low oxygen-enhancement ratio (OER) relative to that for x and $\gamma$ rays. The low OER occurs predominately in the high-dose region of the pion beam in tissue and thus may overcome the resistance of the hypoxic cell to radiation. This has been postulated to be an important cause of failure in the attempt to cure some cancers by conventional radiotherapy.[1]

## II. PION PRODUCTION AND TRANSPORT

The $\pi$ mesons are secondary particles produced in a nuclear reaction. At LAMPF, pions are produced by bombarding a 17.6-g/cm$^2$ graphite target ($\rho = 2.2$ g/cm$^3$) with 760-MeV protons. Negative, positive, and neutral pions ($\pi^-$, $\pi^+$, $\pi^0$) are produced in the proton–carbon collisions. The neutral pions have lifetimes of $10^{-16}$ sec and decay into two $\gamma$ rays. The charged pions have a lifetime of $2.55 \times 10^{-8}$ sec and decay predominately into a muon and a neutrino. The charge of the pion is equal to that of an electron.

The pion biomedical transport channel (Fig. 1) lies in a plane oriented such that the production angle is at 70° to the direction of the proton beam. Some of the $\gamma$ rays from $\pi^0$ decay convert in the target into electron–positron pairs, which have a predominately forward direction. The channel orientation was chosen to reduce the electron component in the beam and still maintain a high-production cross section for pions. The pions are accepted within a solid angle of 16 msr (rms). Negative muons resulting from pion decay in the target region as well as electrons having the appropriate momentum are accepted by the channel with negative pions and remain as contamination in the beam. Muons are also produced throughout the channel by pion decay.

Figure 1 is a view of the bend plane ($X$–$Z$ plane) of the biomedical channel, which consists of eight quadrupole magnets and three wedge-type bending magnets with an intermediate focus between the second and third bends. The total length of the channel is about 11.7 m. The channel opening is filled with three plastic bags containing helium to reduce multiple coulomb scattering. The tuning of the channel has been described by Paciotti *et al.*[2]

## III. PION INTERACTIONS

When negative pions stop in tissue they may be captured by a carbon, nitrogen, or oxygen atom. A capture by hydrogen is quickly transferred to a heavier atom. When the $\pi^-$ is absorbed by the nucleus, approximately 40 MeV of its 140-MeV rest mass is used in overcoming the nuclear binding energy; the remaining 100 MeV appears in the form of kinetic energy of nuclear fragments. About 40 MeV appears in the form of kinetic energy of charged particles such as protons, alpha particles, and heavier recoils that are absorbed locally; the rest (nearly 60 MeV) appears in the form of kinetic energy of neutrons. About 90% of the total energy available from charged particles produced directly by $\pi^-$ capture is deposited within a distance of 2 cm from the capture site. At larger distances these particles contribute less, while the energy deposited by neutrons becomes dominant.[3] A few percent of capture events produce high-energy $\gamma$ rays.


Copyright © 1977 Am. Assoc. Phys. Med.

00133501.001

1087359

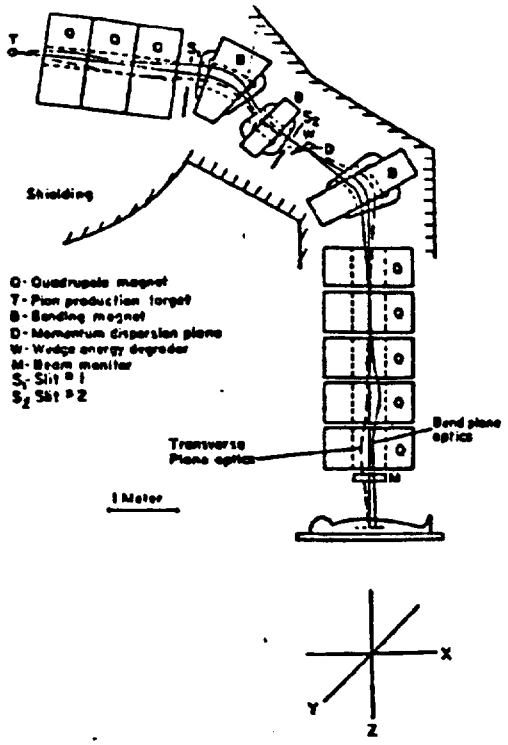


FIG. 1. The LAMPF pion transport channel.

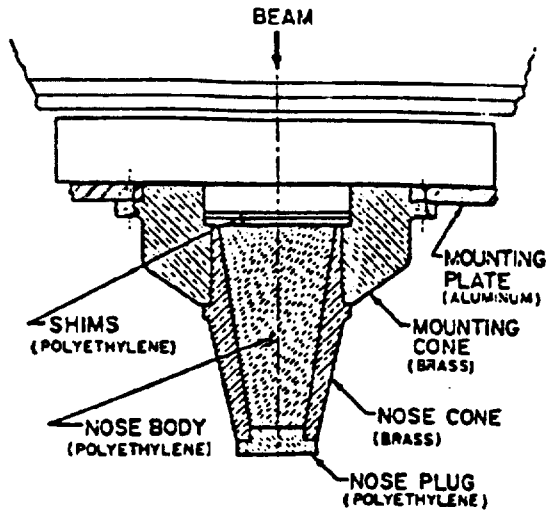


FIG. 2. Treatment cone for skin nodules and superficial tumors.

The unique capture process for negative pions enhances the dose near the Bragg peak region due to the production of short range and heavily ionizing fragments. It is this feature that makes negative pions physically and biologically promising in radiotherapy. In tissue, approximately 73% of the pions are captured in oxygen, 20% in carbon, 3% in nitrogen, and 4% in heavier atoms. The cross sections for heavy ion production (including alpha particles) are significantly different for oxygen and carbon, with more energy per ion for captures on carbon. Therefore the relative abundances of these elements are an important consideration when selecting pion dosimetry materials.

## IV. METHODS AND MATERIALS

All dosimetry measurements reported here were made with small- (~0.1 $cm^3$) thimble ion chambers in a water phantom. The chambers are made by EG&G,[4] have walls made of Shonka A-150 plastic,[5] and are filled with tissue-equivalent (TE) gas. The fractional composition by weight of the TE plastic and gas compared to that of muscle has been reported previously.[6] Shonka A-150 plastic contains an excess of carbon and a depletion of oxygen as compared to muscle in order to make the chamber wall conductive.

The ionization chamber is positioned automatically by a three-dimensional scanner controlled by a PDP-11/45 computer. Computer codes provide for linear, planar, or three-dimensional scans which may be taken in steps as small as 0.1 mm. Any number of readings may be taken at each point. If the spread in the data falls outside the set variance, the readings are repeated. A continuous display of the data in graphical form allows the physicist to observe data acquisition and change scan parameters during the measurement.

The current from the ionization chamber is integrated by a Cary 14 electrometer. ORTEC current digitizers monitor back-to-back transmission ionization chambers in the beam line, which control the exposures. These transmission chambers are filled with continuously flowing argon gas.

## V. DOSIMETRY

Dosimetric measurements have been made for beams used to treat three types of tumors: (1) skin nodules, (2) superficial tumors, and (3) deep-seated tumors. For the first two types, the beam shaping and collimation was done by using the energy-degrading collimator cone shown in Fig. 2. This brass nose cone was designed to stop completely the pions outside the desired treatment volume. The peak of the pion depth-dose distribution was placed at the desired depth by adjusting the thickness of polyethylene absorber. Figure 3 shows a typical beam used for the treatment of skin nodules. The left side of the graph shows the central-axis depth distribution of the ionization resulting from 165-MeV/C pions ($E$ = 76.5 MeV) incident upon a 4-cm-diameter cone. The polyethylene absorber thickness was adjusted so that the end of the nose plug (skin surface) was at point 0.5 cm past the maximum

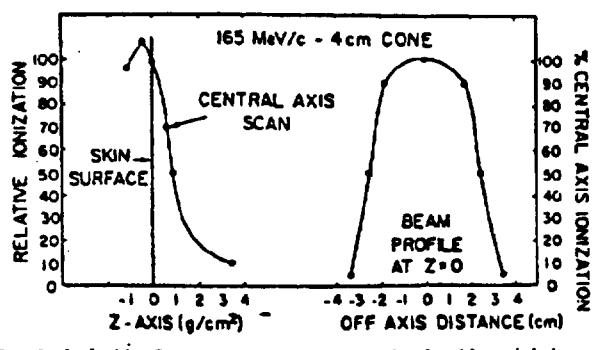


FIG. 3. Left side: Central-axis depth distribution for skin nodule beam. $z$ = 0 is at skin surface. Right side: typical beam profile taken at $z$ = 0.

COPIED FOR HSPT



00133501.002

1087360

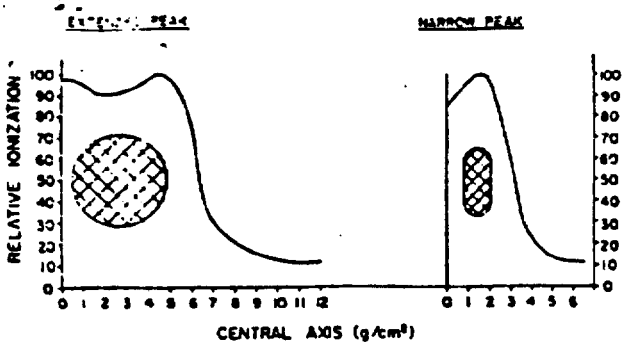


FIG. 4. Central-axis depth distribution for beams used to treat superficial tumors.

of the Bragg peak. This region of the peak is the region of highest linear energy transfer (LET) resulting from the heavy-particle component of the pion capture reaction. A typical beam profile taken along the $Y$ axis of Fig. 1 at $Z = 0$ is shown on the right side of Fig. 3.

These scans were taken in a water phantom. The correct thickness of polyethylene shims needed to place the peak at the desired depth was calculated, then verified by additional measurements.

Figure 4 shows typical central-axis depth distributions for beams designed to treat larger (up to $5 \times 5 \times 5$ cm$^3$) tumors lying at shallow depths below the skin surface. The beam tune and collimator for these beams were the same as for the skin nodule beam but a different wedge degrader (see Fig. 1) was used at the momentum focus of the channel, changing the momentum spread from $\Delta P/P \simeq 2.0\%$ to $\Delta P/P \simeq 4.5\%$ (rms). The larger momentum spread produced an extended peak by spreading the stopping pions over a greater distance. The distribution on the left is the widest spread resulting from this particular wedge degrader. To achieve narrower peaks for smaller lesions, such as shown on the right of Fig. 4, momentum defining slits ($S_2$ in Fig. 1) were adjusted to obtain peak dimensions consistent with the size of the tumor to be treated. The beam profiles for these beams were much the same as the profile shown in Fig. 3.

The distribution of LET is not homogeneous in the Bragg peak of pion beams. Very high LET occurs predominately in the distal portion of the peak resulting in a nonuniform relative biological effectiveness (RBE) across the peak. This is shown in Fig. 5; the low-, medium-, and high-LET components of the extended peak are superimposed upon the extended peak distribution of Fig. 4. The low-LET component is composed mostly of pions and electrons, the medium-LET component is due mainly to protons, deuterons, and tritons, and the high-LET component is comprised of alpha particles and heavy recoils. These distributions were measured with thin silicon detectors which are capable of resolving the various groups of charged particles.[7] The dose in the proximal region of the peak has less high- and medium-LET components than the dose in the distal region. Therefore, patient treatments using this particular beam were performed by shifting the extended peak across the tumor volume and adjusting the tumor dose for each application to achieve a uniform biological effect. The results of this treatment technique have been reported previously.[8]

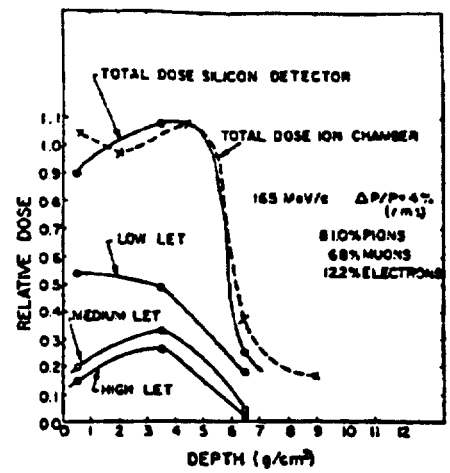


FIG. 5. Silicon-detector measurements of the total dose and the low-, medium-, and high-LET dose components (solid lines), and the total dose measured by ion chamber (dashed line).

Four basic beams have been developed for the treatment of deep-seated tumors; the central-axis depth profiles for these beams are shown in Fig. 6. These curves have been normalized to 100% at the maximum peak dose. There are three interesting features of these curves: (1) As the depth of penetration increases, the width of the Bragg peak is broadened because the percentage momentum spread is roughly constant, independent of energy; (2) the deeper penetrating beams have a smaller peak-to-plateau ratio, since the peak is spread more due to range differences of the incoming momentum distribution; (3) the dose in the region beyond the Bragg peak (~10%) is due mostly to the higher-energy muons and electrons, which have ranges greater than pions of the same momentum, but there is also some contribution from protons and neutrons. The spacing of the beam momenta was chosen such that the entire range of depths from 0 to 27 cm could be reached by adding polyethylene in the beam to shift the peak of each beam to shallower depths. These curves were measured underneath a rangeshifter (discussed below) which has an equivalent water thickness of approximately 3.0 g/cm$^2$ at its minimum position. Thus, the range in water for these beams is 3.0 cm more than shown in Fig. 6.

The narrow peaks of these beams are spread with a rangeshifter to achieve larger treatment volumes. The

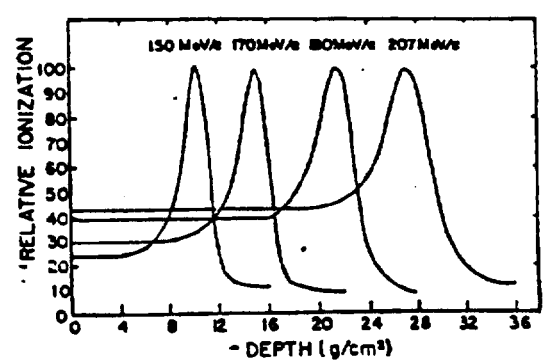


FIG. 6. Central-axis depth profiles for basic beams used to treat deep-seated tumors.

COPIED FOR HSPT



00133501.003
1087361

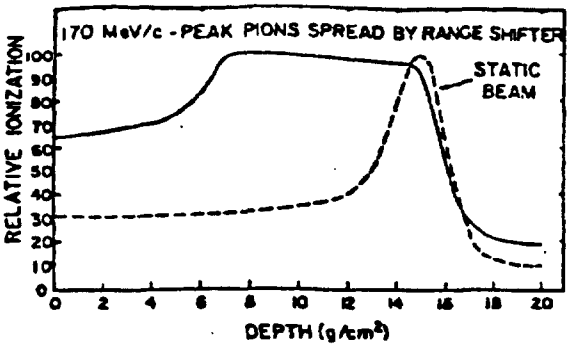


FIG. 7. Example of a Bragg peak (dashed line) spread to 8 cm using the rangeshifter (solid line).

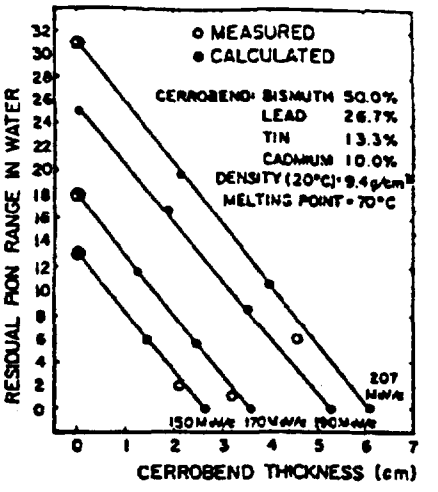


FIG. 9. Calculated (closed circles) and measured (open circles) residual pion range in water versus thickness of alloy used for collimation.

rangeshifter is computer controlled and can be programmed to produce peaks varying in dimension from the width of the static peaks shown in Fig. 6 to widths up to 15 cm. Figure 7 shows a typical spread peak produced by the rangeshifter. This peak is spread over 8 cm and is flat within 5% over the entire peak. The rangeshifter produced these distributions by varying the height of a column of fluid in the beam path so as to superimpose a large number of static peaks over the desired width.

The spread peaks have a nonuniform distribution of LET, hence RBE, across the peak. The rangeshifter can be used to modify the peak dose to produce a uniform biological effect, as shown in Fig. 8. The analytical rangeshifter function to do this was developed from preliminary radiobiology data, which indicated that the RBE was 1.0 in the proximal region of the peak and was 1.4 in the distal region. Assuming a linear RBE increase across the peak, the resulting "biologically flat" beam shown by the dashed curve of Fig. 8 was produced. The analytical function can be changed readily as the radiobiological data become more complete. The rangeshifter and the derivation of the analytical functions are discussed in detail elsewhere.[9]

Treatment cones, such as the one in Fig. 2, are not practical for the large-volume beam tunes. Currently, collimators made from a low-melting-point alloy are being tested. The advantage of this alloy is that it is rather dense ($\rho = 9.4$ g/cm$^3$) and can be easily formed into collimators of highly irregular shapes. Calculations were made to determine the correct thickness of the alloy required to stop completely the pions from each beam tune. These calculations weighted the pion stopping power for the components in the alloy (50.0% bismuth, 26.7% lead, 13.3% tin, and 10.0% cadmium). The calculations were then verified by experiment; and a comparison of calculation versus experimental data is shown in Fig. 9.

The effect of the alloy collimators on the pion beam is exemplified in Fig. 10, which shows a typical $x$ profile of the beam taken in the center of a peak spread 8 cm in depth underneath a 9-cm × 7-cm elliptical collimator, 3 cm thick. The collimators are most effective when placed at the surface of the phantom with the rangeshifter directly above and in physical contact with the upper-collimator surface. The shape of the beam profiles varies considerably with depth in phantom. At the surface ($z = 0$) directly under the collimator, the plateau profile is very flat with almost perpendicular falloff on the edges. In the peak region, the profiles diminish in flatness as the depth increases, as shown in Fig. 11. At the 80% level, the distal peak profile is 6.4 cm wide compared to a width of 7.8 cm at the same level for the profile taken in the proximal peak. The profile shapes will also change depending on which beam tune is used, being flatter and sharper for the beams which have shallower penetration due to less multiple coulomb scattering.

A typical isoionization distribution for the 170-MeV/C pion 8-cm-spread peak is shown in Fig. 12. The penumbra

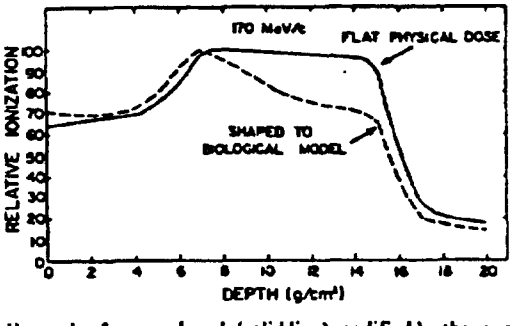


FIG. 8. Example of a spread peak (solid line) modified by the rangeshifter to give a uniform biological effect (dashed line).

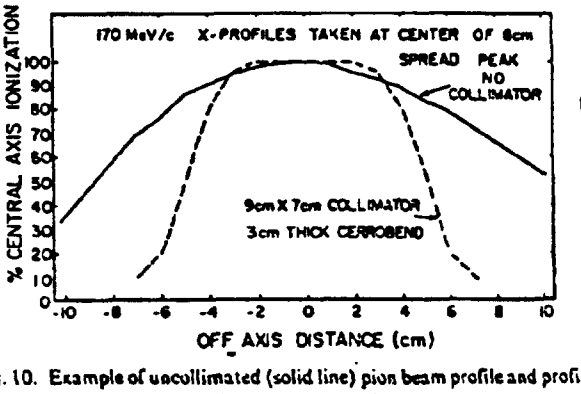


FIG. 10. Example of uncollimated (solid line) pion beam profile and profile of collimated beam (dashed line) using alloy (Cerrobend).

COPIED FOR HSPT



00133501.004

1087362

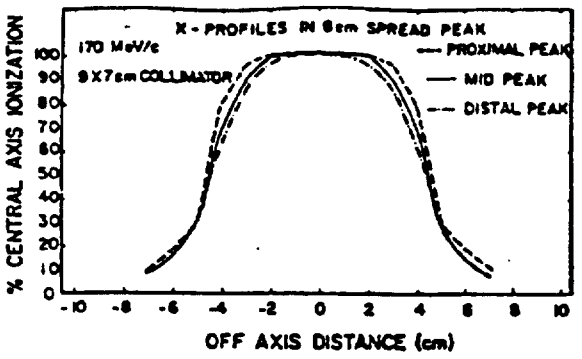


FIG. 11. Beam profiles of collimated pion beam taken in the proximal peak (dashed line), med peak (solid line), and distal peak (dash-dot line) of an 8-cm-spread peak.

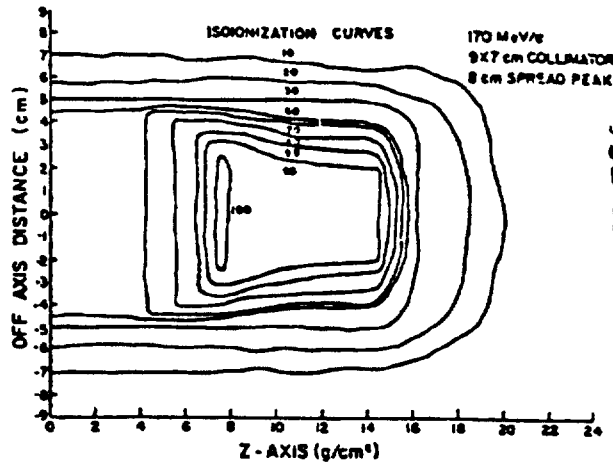


FIG. 12. Isoionization distribution of 170-MeV/C collimated pion beam with peak spread to 8 cm.

COPIED FOR HSPT

for this distribution is wide for a number of reasons: (1) pion multiple scattering; (2) the optimum collimator edge geometry with respect to pion multiple scattering has yet to be determined; (3) the ionization measurements have not been converted to absorbed dose; (4) the collimators are not effective in stopping the high-energy muons and electrons in the beam; and (5) the fast neutrons produced in the capture process contribute significantly to the dose in this region.[3,10] This beam is composed of 81.7% pions, 6.6% muons, and 11.7% electrons.

## VI. PION ABSORBED-DOSE CALCULATIONS

The pion distributions that have been presented in this paper have been given in terms of ionization produced in the thimble chamber because the conversion from ionization to absorbed dose in the pion beam has not been completed. The difficulty is due primarily to the complex secondary charged-particle fluence generated in the chamber wall. The problem is compounded by the fact that the charged-particle fluence varies greatly between the peak and plateau regions of the beam and even in the peak itself due to nonuniform distributions of star events. Pion interactions in the wall material produce electrons, protons, deuterons, tritons, alpha particles, and heavy recoils which in turn produce ionization in the TE gas volume. In addition, ionizations in the gas volume are also produced by primary pions, muons, and electrons. In order to give a complete physical characterization of the energy deposition in the gas, it is necessary to know accurately the fluence and energy spectra of all the secondary charged particles and the primary pions. These data are not available at this time; however, experiments are being designed that will provide this information.

Presently it is assumed that the thimble ion chamber acts as a Bragg-Gray cavity in the pion beam and the dose in muscle is calculated using the Bragg-Gray relation.[6] Because of the lack of detailed knowledge of the energy deposition events, certain assumptions have been made concerning the secondary charged particles in order to calculate the effective energy required to produce an ion pair in the gas ($W$) and the average mass-stopping-power ratio. These calculations are in a preliminary stage and the results subject to revision; hence, they will not be presented here. A kerma correction is applied to the dose calculated by the Bragg-Gray equation to transform the dose from the TE plastic chamber wall to absorbed dose in muscle. This correction is principally due to the difference in the cross sections for heavy-ion production in oxygen and carbon and is deduced from measured data and calculations.[3,11]

A program of experimental investigations and Monte Carlo calculations is now being undertaken to provide the necessary information to permit the statement of absorbed dose in all regions of the pion beams. The present statement of pion absorbed dose has a minimum uncertainty of ±10% and, in fact, may be in error by as much as ±20%, depending on the assumptions made and the applicability of the Bragg-Gray theory to pion beams.

## VII. SUMMARY

The dosimetry of the LAMPF pion therapy beam has been discussed. This dosimetry is in the early stages of development and much work needs to be done before it is considered complete. The major problems are the collimation of pion beams and the lack of detailed knowledge of the exact particle fluence and energy spectra in both the plateau and peak regions of the beam.

In the near future scanning pion beams will be developed which will have much sharper edges and higher dose rates than the beams presented in this report.

## ACKNOWLEDGMENT

These investigations were supported in part by U.S. Public Health Service Grants CA-16127 and CA-14502 from the National Cancer Institute, Division of Research Resources and Centers, and by the U.S. Energy Research and Development Administration.

[1] L. G. Gray, Am. J. Roentgenol. 85, 803 (1961).
[2] M. A. Paciotti, J. N. Bradbury, J. A. Helland, R. L. Hutson, E. A. Knapp, O. M. Rivera, H. B. Knowles, and G. W. Pfeuffer, IEEE Trans. Nucl. Sci. NS-22, 1784 (1975).
[3] J. R. Dutrannois, R. N. Hamm, J. E. Turner, and H. A. Wright, Phys. Med. Biol. 17, 765 (1972).
[4] EG&G Inc., Santa Barbara Division, Goleta, CA 93017.



00133501.005

1087363

[5]F. R. Shonka, J. E. Rose, and G. Failla. Paper No. P/753. *Geneva Conference on Progress in Nuclear Energy, Series XII*, London, Oxford, Vol. I, pp. 160–166 (1959).

[6]A. R. Smith, P. R. Almond, J. B. Smathers, V. A. Otte, F. H. Attix, R. B. Theus, P. Wixson, H. Bichsel, J. Eenmaa, D. Williams, D. K. Bewley, and C. J. Parnell. Med. Phys. 2, 195 (1975).

[7]C. Richman. Radiat. Res. 66, 453 (1976).

[8]A. R. Smith, M. M. Kligerman, C. A. Kelsey, R. G. Lane, P. A. Berardo, M. A. Paciotti, and C. Richman. Int. J. Radiat. Oncol. Biol. Phys. (1976).

[9]H. I. Amols, D. J. Liska, and J. Halbig, "The use of a Dynamic Rangeshifter for modifying the Depth Dose Distribution of Negative Pions," presented at RSNA-AAPM Meeting, Chicago, 1976; Med. Phys. 4, 404 (1977).

[10]M. E. Schillaci and D. L. Roeder. Phys. Med. Biol. 6, 821 (1973).

[11]J. Baarli and A. H. Sullivan. *Dosimetric Problems of Negative pi Mesons*, XIIIth Int. Congr. Radiol., Madrid, Spain (1973), Vol. 2, pp. 426–431.

COPIED FOR
HSPT



00133501.006

1087364